L08

Proceedings of the 5th International Conference on Inverse Problems in Engineering: Theory and Practice, Cambridge, UK, 11-15th July 2005

A NEW INVERSE SOLVER FOR DIFFUSION TOMOGRAPHY USING MULTIPLE SOURCES

T. R. LUCAS[1]
[1] *Department of Mathematics, University of North Carolina at Charlotte, Charlotte, NC, 28223, USA*
e-mail: trlucas@uncc.edu

Abstract - This is a preliminary report on the development of a diffusion based inverse solver for the Helmholtz equation in the frequency domain, in the context of optical tomography. This utilizes a great simplification of the previously developed Elliptical Systems Method with the use of a certain new PDE of the 2nd order, with related boundary and special conditions. In this report we consider the recovery of just the absorption coefficient with both theory and numerical examples, focusing on the case of incomplete data collection using multiple continuous wave (zero frequency) sources. The incomplete data collection is over a rectangular region and includes use of sources and detectors limited to the top and bottom sides, detectors on the transmitted sides only and detectors on the back-reflected sides only.

1. INTRODUCTION

It is common in applied work in engineering such as the search for buried land mines, or in medical imaging for diagnosis of possible breast tumors, to have only limited boundary measurement data, back reflected in the first case or transmitted in the second. Here we formulate the problem as one of coefficient recovery from incomplete boundary data in inverse problems. In this work we are using a diffusion partial differential equation (PDE) as an approximation for the more accurate transport PDE [2].

The Elliptic Systems Methods (ESM) was originally introduced [8] for the solution of the time dependent diffusion equation using time dependent data with just one source, but many detectors. One of the notable advantages of this whole family of methods is that they use a differential form as contrasted to an integral form, which leads to sparse matrix systems instead of full ones, with obvious computational advantages. Many experiments, including the case of incomplete data collection, were reported in [9]-[10]. In the ESM the inverse problem is reduced to a system of overdetermined second order boundary value problems, with the time variable integrated out using Legendre polynomials, in effect using a truncated generalized Fourier series. As one approach to resolve this over-determination, a fourth order biharmonic equation was introduced to provide a well-posed problem. In [8]-[10] the 4^{th}-order elliptic system was solved by using a mixed form of the finite element method (FEM), splitting the system into two adjoint systems of 2^{nd}-order PDE's which were then solved using quadratic elements over triangles. With the most standard number of such Legendre polynomials being four, this led to a coupled system of eight 2^{nd} order PDE's. Recently in [13] an improved implementation of this method has been developed which, among other improvements, directly solves the 4^{th}-order biharmonic type system with Bogner-Fox-Schmit bi-cubic elements [4] using the FEM over rectangles. This led to a coupled system of four 4^{th} order PDE's, in the form of generalized biharmonics, which has given improved coefficient recovery results.

Also the ESM has been extended [11] to applications involving the search for near surface land mines, with the source in the form of ground penetrating radar, leading to the use of back-reflected data. In this original 2^{nd} generation improvement of the ESM, the resulting equations are still solved *indirectly* but without the complicating need to introduce truncated Fourier series. A second innovation was a major improvement in the approach used to solve for the material properties (absorption and diffusion coefficients) using the measured (or simulated) data readings, by adding this data to the original system, and using this overdetermined form to recover the material properties though an iterative process in frequency. This allowed staying with the 2^{nd} order formulation, although an integro-differential equation with a Volterra-like integral was required. This integro-differential equation was the price paid for allowing a differentiation to temporarily eliminate the unknown coefficient, similar in many ways to [8]. Finally in [12] a notable improvement was made that eliminated the need for this complicating factor, the integro-differential equation, allowing for a direct solution.

In this paper we are generalizing the results of [12] to the diffusion process [2] in the frequency domain. The main complicating factor is that the source is an *internal* point source rather then an *exterior* plane wave, and the practical need to go from the two data sets used on the air/soil boundary in

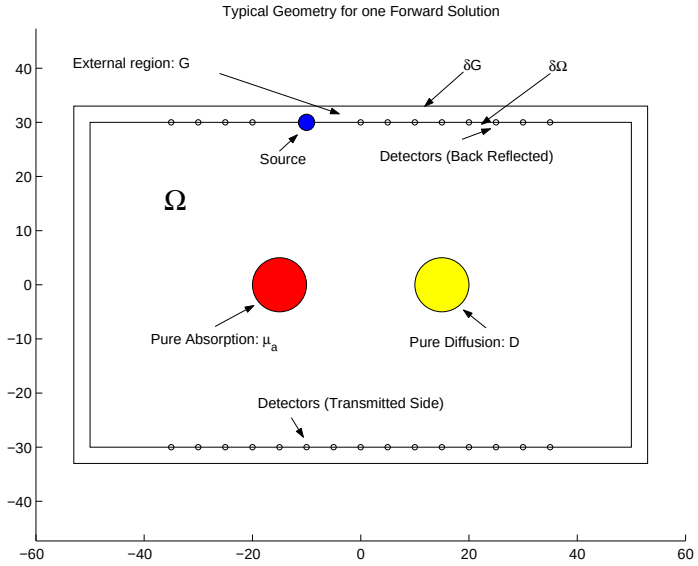

Figure 1: General setup for external and internal regions.

[11]-[12] to just *one* incomplete data set. In this paper we are developing for the first time with the ESM family of methods, an approach that allows for the use of many sources (and also if we wished many frequencies), and incorporates the many advantages of [12]. In this development we can use a mixture of many kinds of incomplete data: data on some sides alone, transmitted data alone or back-reflected data, or any combination.

The plan for this paper is that in Section 2 we will explain the physical problem and the Helmholtz equation used to model it. In Section 3 effective solution methods to solve the forward problem are explained. The new inverse solver for this diffusion process will be introduced in Section 4, and slightly expanded on in Section 5.3. Of primary interest in Section 4 are the treatments of the internal source term and the boundary conditions (BC's). Some computational details and speed-ups are given in Section 5. Section 6 contains numerical examples, mostly using incomplete data sets, with some conclusions in Section 7.

2. PHYSICAL PROBLEM AND MODEL

We begin by modelling the propagation of light in human tissue as a diffusion process in the frequency domain [2], see Figure 1. Consider a domain Ω with boundary $\partial\Omega$, a modulated frequency ω and a source at location $\mathbf{x_0}$. We will refer to this as the physical domain. We shall assume that the values for absorption a_0 and diffusion D are constant, except for certain small inclusions inside Ω away from the boundary $\partial\Omega$ with variable absorption and/or diffusion, as shown in Figure 1. This can be modelled [1] by the complex Helmholtz equation:

$$-\nabla\cdot(D(\mathbf{x})\nabla u(\mathbf{x}))+\left(a(\mathbf{x})+\frac{i\omega}{c}\right)u(\mathbf{x}) \;=\; \delta(\mathbf{x}-\mathbf{x}_0)\quad \mathbf{x}\in G \tag{1}$$

$$u(\mathbf{x}) \;=\; 0,\quad \mathbf{x}\in\partial G \tag{2}$$

over a certain extended domain G with homogeneous Dirichlet BC's on ∂G. We will refer to the domain G as the computational domain, and as will be seen we will solve not only this forward problem over G, but also the related inverse problem of recovering the inclusion values. In this preliminary report we consider the recovery of just the absorption coefficient $a(\mathbf{x})$, so $D(x)\equiv D$ is constant over Ω. We nevertheless display D throughout in a way that easily allows for future generalizations. It should also be noted [2] that the diffusion coefficient has a dependency on absorption. However for media low in absorption compared with scattering such as are simulated here, this dependency is sufficiently small as to justify ignoring it. Finally, while the theory developed here will be applicable to both variable source positions and variable frequencies, this report will simulate only the continuous wave (CW) case where the frequency $\omega = 0$.

3. FORWARD PROBLEM

The solution must be calculated for each source/frequency pair and tabulated at each detector position. We place this data in tables representing the top, bottom, left and right sides for detector data (complex values), and later use selected subsets. There were two approaches we considered for solving the forward problem (1-2):

3.1 DIRECT SOLUTION APPROACH

Here we use a direct solution of (1-2). For our solution method we used the FEM with FEMLAB [5]. This worked well, and using the weak form for the impulse function was straightforward. Since we were solving for many sources, it was critical that for each run to introduce a node point (vertex) at the current source position. This would be exchanged with each new source position.

3.2 ANOMALOUS EQUATION APPROACH

We have found that a particularly effective computational method for the forward problem, being both rather simple computationally and avoiding any difficulties from the interior unit impulse function $\delta(\mathbf{x}-\mathbf{x}_0)$, is to solve for the difference

$$v(\mathbf{x}) = u(\mathbf{x}) - u_0(\mathbf{x}),$$

where $u(\mathbf{x})$ is the solution to a new problem with perturbed absorption values $a(\mathbf{x}) = a_0 + \Delta a(\mathbf{x})$ with $\Delta a(\mathbf{x})$ being the perturbed value of the constant absorption value a_0. The PDE that generates $v(\mathbf{x})$ is:

$$-\nabla \cdot D\nabla v(\mathbf{x}) + \left(a(\mathbf{x}) + \frac{i\omega}{c}\right) v(\mathbf{x}) = -\Delta a(\mathbf{x}) \cdot u_0(\mathbf{x}) \tag{3}$$

and $x \in G$ with the BC: $v(x) = 0$, $x \in \partial G$ as before. The homogeneous solution $u_0(x)$ thus only needs to be evaluated inside the inclusions, as elsewhere $\Delta a(\mathbf{x})$ is zero. Here and elsewhere we efficiently evaluate the homogeneous solution $u_0(\mathbf{x})$ by the *method of images*, a series type method, which quickly generates an arbitrarily accurate solution.

The derivation of the anomalous equation is straightforward: Let $u(x)$ be the solution of a Helmholtz equation with a perturbed absorption $a(\mathbf{x})$ and $u_0(x)$ be the solution of the original PDE with constant diffusion and absorption terms D and a_0. Thus:

$$-\nabla \cdot D\nabla u_0(\mathbf{x}) + \left(a_0 + \frac{i\omega}{c}\right) u_0(\mathbf{x}) = \delta(\mathbf{x}-\mathbf{x}_0)$$

$$-\nabla \cdot D\nabla u(\mathbf{x}) + \left(a(\mathbf{x}) + \frac{i\omega}{c}\right) u(\mathbf{x}) = \delta(\mathbf{x}-\mathbf{x}_0)$$

with BC's $u(\mathbf{x}) = u_0(\mathbf{x}) = 0$ for $x \in \partial G$. Letting $u(\mathbf{x}) = u_0(\mathbf{x}) + v(\mathbf{x})$, $a(\mathbf{x}) = a_0 + \Delta a(\mathbf{x})$ and subtracting gives:

$$-\nabla \cdot D\nabla v(\mathbf{x}) + \left(a(\mathbf{x}) + \frac{i\omega}{c}\right) v(\mathbf{x}) + \Delta a(\mathbf{x}) u_0(\mathbf{x}) = 0$$

which immediately yields the **anomalous equation** (3) in $v(\mathbf{x})$, with the BC: $v(x) = 0$, $x \in \partial G$.

The anomalous equation must be solved once for each source and each frequency. Complex valued data is collected at discretely placed detectors along the physical boundary, and stored for later use.

4. INVERSE PROBLEM

We specify the inverse problem as follows to recover the interior absorption coefficient $a(\mathbf{x}) = a_0 + \Delta a(\mathbf{x})$: the known (rectangular) geometry; the constant diffusion term D; the background constant absorption term a_0; the locations x_0 and modulated frequencies ω of a series of point sources of unit impulse strength; and the location and readings from a series of detectors. It is loosely assumed that the perturbations $\Delta a(\mathbf{x})$ are isolated and sufficiently small. Each source can use different sets of modulated frequencies and have readings for detectors on: all sides; just the top and bottom sides; back-reflected data alone; or transmitted data alone. The primary examples will focus on problems with *incomplete data collection*, as illustrated above.

4.1 THE INVERSE SOLVER

The inverse solver developed in this paper is derived by modifying the anomalous equation, using a normalized solution. Consider the change of variable:

$$z(\mathbf{x}, x_0^k, \omega_k) = \frac{v(\mathbf{x}, x_0^k, \omega_k)}{u_0(\mathbf{x}, x_0^k, \omega_k)}. \tag{4}$$

Substituting $v = z \cdot u_0$ into the anomalous equation (3) gives:

$$(-\nabla \cdot D\nabla z)\, u_0 - 2D\nabla u_0 \cdot \nabla z - (\nabla \cdot D\nabla u_0)\, z + \left(a_0 + \Delta a(\mathbf{x}) + \frac{i\omega}{c}\right) z \cdot u_0 = -\Delta a(\mathbf{x}) \cdot u_0.$$

Dividing by u_0 and simplifying gives:

$$-\nabla \cdot D\nabla z - 2D\frac{\nabla u_0}{u_0} \cdot \nabla z + \left(-\nabla \cdot D\nabla u_0 + (a_0 + \frac{i\omega}{c}) \cdot u_0\right) \frac{z}{u_0} + \Delta a(\mathbf{x}) z = -\Delta a(\mathbf{x})$$

Since u_0 satisfies the unperturbed diffusion equation (1) we finally get:

$$-\nabla \cdot D\nabla z - 2D\frac{\nabla u_0}{u_0} \cdot \nabla z + \frac{\delta(\mathbf{x} - \mathbf{x_0})}{u_0} z + \Delta a(\mathbf{x}) z = -\Delta a(\mathbf{x}). \tag{5}$$

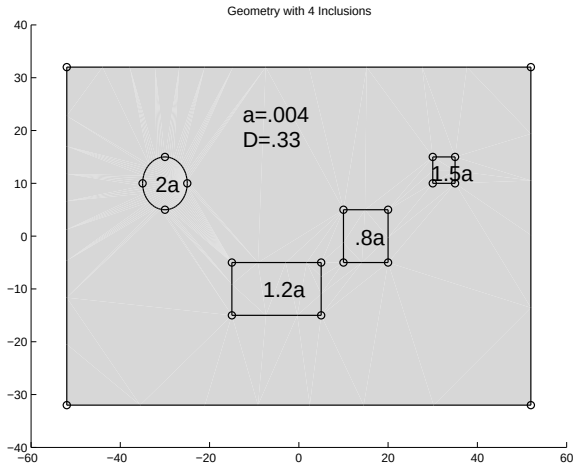

(a) 4 Inclusions of different shapes with $\mathbf{a_0} = \mathbf{.004mm^{-1}}$ perturbed by $\mathbf{a_0}$, $\mathbf{0.2a_0}$, $\mathbf{-0.2a_0}$ and $\mathbf{0.5a_0}$.

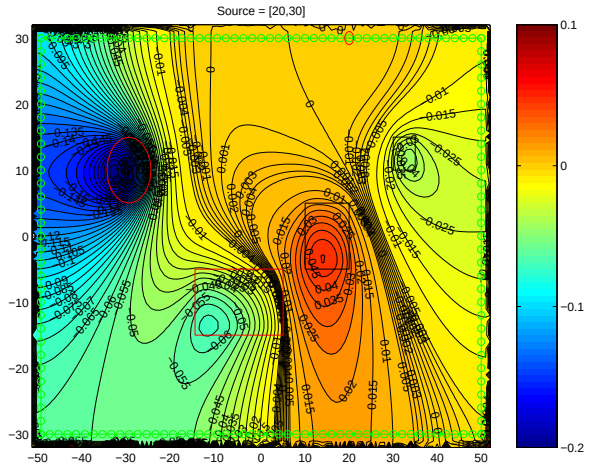

(b) Information rich plot of the *normalized* perturbation $z = \frac{v}{u_0}$ of the photon density.

Figure 2: (a) Inclusion configuration showing $a(x) = a_0 + \Delta a$ and (b) Plot of z for a source located at $(20, 30)mm$ for a medium with the previous 4 inclusions using $\omega = 0$ (CW case).

The above substitution $z = \dfrac{v}{u_0}$ has been part of this family of methods for many years [8]-[13]. In Figure 2b this function is plotted. In this plot the advantage of using such a normalized perturbataion is clear, as it changes rapidly around all of the inclusions, unlike for example the original perturbation, whose primary change is around just those inclusions close to the source. We are now ready to resolve two key questions: what to do with the unit impulse term $\delta(\mathbf{x} - \mathbf{x_0})$ and what to use for the boundary conditions? Since $\delta(\mathbf{x} - \mathbf{x_0})$ is zero for all $\mathbf{x}$ except for the source position, and since clearly z must be zero at the source $\mathbf{x_0}$, due to the singularity in u_0, our approach is to omit the term with $\delta(\mathbf{x} - \mathbf{x_0})$, and add the auxiliary condition that at the source $\mathbf{x_0}$, $z(\mathbf{x_0}) = 0$.

A visual inspection of Figure 2b with the *computed* values $z = \frac{v}{u_0}$, where $v(\mathbf{x})$ was computed from the original anomalous equation using the inclusion values of Figure 2a, and $u_0(\mathbf{x})$ was computed by the method of images, showed contours that appear orthogonal to the boundary throughout the domain. This would suggest that $\frac{\partial z}{\partial n} = 0$ at least to a significant level of approximation. A second order expansion

of $\frac{\partial z}{\partial n}$ on the boundary of the domain (where both $u_0(\mathbf{x}) = 0$ and $v(\mathbf{x}) = 0$) indeed gives the following approximation for $\frac{\partial z}{\partial n}$:

$$\frac{\partial\left(\frac{v}{u_0}\right)}{\partial n} = \frac{u_0\frac{\partial v}{\partial n} - v\frac{\partial u_0}{\partial n}}{u_0^2} \approx \frac{\frac{1}{2}\left[\frac{\partial u_0}{\partial n}\frac{\partial^2 v}{\partial n^2} - \frac{\partial^2 u_0}{\partial n^2}\frac{\partial v}{\partial n}\right]}{\left(\frac{\partial u_0}{\partial n}\right)^2}$$

which both explains the consistent visual observations, and confirms the approximation since the partial derivatives of v are in general very much smaller than $\frac{\partial u_0}{\partial n}$. Thus we will use as the boundary condition for the normalized anomalous equation: $\frac{\partial z}{\partial n}\,|_{\partial G} = 0$. A similar equation was used in the time-dependent studies [8]-[10],[13]. We can now summarize our formulation of the normalized anomalous equation, for the source at $\mathbf{x} = \mathbf{x_0}$:

$$-\nabla \cdot D\nabla z - 2D\frac{\nabla u_0}{u_0} \cdot \nabla z + \Delta a(\mathbf{x})z = -\Delta a(\mathbf{x}) \text{ for } x \in G\backslash\mathbf{x_0} \tag{6}$$

$$\frac{\partial z}{\partial n}\,|_{\partial G} = 0 \tag{7}$$

$$z(\mathbf{x_0}) = 0 \tag{8}$$

While not exact due to the approximation in the BC's, this system gives good results as long as $\frac{\partial v}{\partial n}$ and $\frac{\partial^2 v}{\partial n^2}$ are slowly changing near ∂G. This should be the case when there is a homogeneous band of constant values of $a(x)$ near the boundary ∂G.

We will now use over-determined data from a series of physical measurements (or computer simulations) with varying sources and modulated frequencies to turn the above formula into an iterative inverse solver. For each source $\mathbf{x_0^k}$ with modulated frequency ω_k let $u_0^k = u_0(\mathbf{x}, x_0^k, \omega_k)$ and consider the overdetermined systems:

$$-\nabla \cdot D\nabla z_k - 2D\frac{\nabla u_0^k}{u_0^k} \cdot \nabla z_k + \Delta a_k(\mathbf{x})z_k = -\Delta a_k(\mathbf{x}) \text{ for x} \in G\backslash\mathbf{x_0^k} \tag{9}$$

$$\frac{\partial z_k(\mathbf{x})}{\partial n} = 0, \quad \mathbf{x} \in \partial G \tag{10}$$

$$z_k(\mathbf{x_0^k}) = 0 \tag{11}$$

$$z_k(\mathbf{x}, x_0^k, \omega_k) = f(\mathbf{x}, x_0^k, \omega_k), \quad x \in \Gamma^k \tag{12}$$

where $f(\mathbf{x}, x_0^k, \omega_k) = \frac{\hat{u}(\mathbf{x}, x_0^k, \omega_k) - u_0(\mathbf{x}, x_0^k, \omega_k)}{u_0(\mathbf{x}, x_0^k, \omega_k)}$ and $\hat{u}$ represents data at mesh points $\mathbf{x}$ along those parts of the physical boundary Γ^k where data is collected from detector readings or from the simulations (forward runs) of this paper, and expanded for example by smoothing and interpolation. Note that Γ^k will in general vary with k, for example in the case of transmitted data, Γ^k would be that part of $\partial\Omega$ opposite the source x_0^k.

Begin with $k = 1$ and $\Delta a_1(\mathbf{x}) \equiv 0$. Iterate (9-12) repeatedly using the various sources and modulated frequencies, updating over the physical region by

$$\Delta a_{k+1}(\mathbf{x}) = \nabla \cdot D\nabla z_k + 2D\frac{\nabla u_0}{u_0} \cdot \nabla z_k - \Delta a_k(\mathbf{x})z_k \tag{13}$$

or

$$\Delta a_{k+1}(\mathbf{x}) = \left(\nabla \cdot D\nabla z_k + 2D\frac{\nabla u_0}{u_0} \cdot \nabla z_k\right)/(1 + z_k). \tag{14}$$

In preliminary studies we have found no particular differences between the results using either the more conservative (13) or the more aggressive (14) formula above.

4.2 ALGORITHM FOR THE INVERSE SOLVER

The work of the previous section can be encapsulated as an algorithm as follows:

1. Include grid points for the FEM mesh along the physical boundary, at least where data is available.
2. For each source/frequency pair (x_0^k, ω_k), $k = 1..N_k$, construct the function $f(\mathbf{x}, x_0^k, \omega_k)$.

3. Set the initial perturbation term $\Delta a_1(\mathbf{x}) = 0$.
4. Make P passes, $p = 1, 2, ...P$
5. For $k = 1, 2, ...N_k$
   Solve (9-12) for z_k, using the normal equations method (See Section 5.2)
   Use (13 or 14) to calculate Δa_{k+1}
   End For
   Set $\Delta a_1(\mathbf{x}) = \Delta a_{N_k+1}(\mathbf{x})$
   End passes

In Section 5.3 we shall refer to this method as the *sequential solution method*, where the perturbation is updated after each z solve. An alternative method, called averaging is proposed there, and the approaches can be mixed from pass to pass.

5. COMPUTATIONAL APPROACH AND SOME SPEED-UPS

All of this work was performed using a combination of matlab and FEMLAB [5]. The code for the forward solver (using the anomalous equation approach of Section 3.2) going though many sources (and if desired many frequencies), and outputting values at selected detector locations, was about 300-400 lines. The inverse solver was from 1000-1500 lines, including considerable informative graphics. We have found three major methods of speeding up the computations:

5.1 PRECOMPUTATION OF $\frac{\nabla u_0}{u_0}$

The values of the homogenous solution and the coefficient $\frac{\nabla u_0}{u_0}$ depend solely on the geometry and the constant values D and a_0, and thus can be precomputed. The preferred method is the method of images, extended to this case.

5.2 NORMAL EQUATIONS SOLUTION USING PCG WITH A PRECONDITIONER

On the first pass through the system the least squares matrix for the inverse solver without any inclusion data is evaluated for each value of k. This gives an overdefined linear system of the form $A_k x = b$. The resulting normal equations matrix $A_k^* A_k$ is then evaluated and factored using Cholesky factorization [6], with the resulting factorization being stored to disk. Each time the normal equations matrix is resolved on later passes these factorizations are recalled and used as preconditioners for the preconditioned conjugate (pcg) gradient method [7]. This is similar to the approach used in [12], in that only one preconditioner need be computed for many solutions to nearby systems. This speeds up the solvers by a factor of 30 or so, with accurate solutions typically found in just 3-7 iterations.

5.3 AVERAGING VERSUS SEQUENTIAL

An alternative to the algorithm described in Section 4.2 is to make all computations in one particular pass using a *fixed value* for the estimated inclusions Δa in (9) and also in (13), if the conservative recovery equation is used. Then after each pass average the various results obtained from (13 or 14) over that pass, to obtain the fixed value of Δa for the next pass. This makes the ordering not a factor, and presents the opportunity to perform parallel computations on a Beowulf cluster.

In Section 6 for each example we start with 10 sequential passes followed by 20 averaging passes. An advantage of using the sequential method in the early passes is to approach a reasonable Δa more rapidly. However the averaging approach has so far proven superior in our numerical studies for obtaining a finalized result.

6. NUMERICAL EXAMPLES

All of our examples will attempt inclusion recovery in an otherwise homogeneous region with 4 inclusions as shown and detailed in Figure 2a. For the sample problems we have considered, the computational region was $[-52, 52]mm \times [-32, 32]mm$ and the physical region, with sources and detectors on the boundary, was $[-50, 50]mm \times [-30, 30]mm$. The background absorption $a_0 = .004mm^{-1}$, the constant diffusion $D = .33mm$ and the absorption values inside the four inclusions are as displayed. The grid uses $\Delta x = \Delta y = 2mm$. Various increasingly limited choices of sources and detectors will be made.

All cases but the first will be examples of incomplete data collection (IDC), where the detector locations are on some sides only, depending on where the corresponding source is located. In all four examples presented below the sequential replacement method is used for the first 10 passes, and then averaging is used for 20 more.

6.1 FIRST EXAMPLE: COMPLETE DATA COLLECTION; ALL 4 SIDES

Twelve sources are used with a CW signal ($\omega = 0$): 4 on the top and bottom, 2 on each side. Detectors are placed every 2mm on all four sides of the physical boundary $\partial\Omega$. The matrix solver for the least squares solution on a 3.06 GHz PC takes about 30 seconds a matrix for the first pass, and about .75 seconds/pass for the rest using the pcg method. The results are shown in Figure 3, and appear successful, accurately identifying all four inclusions.

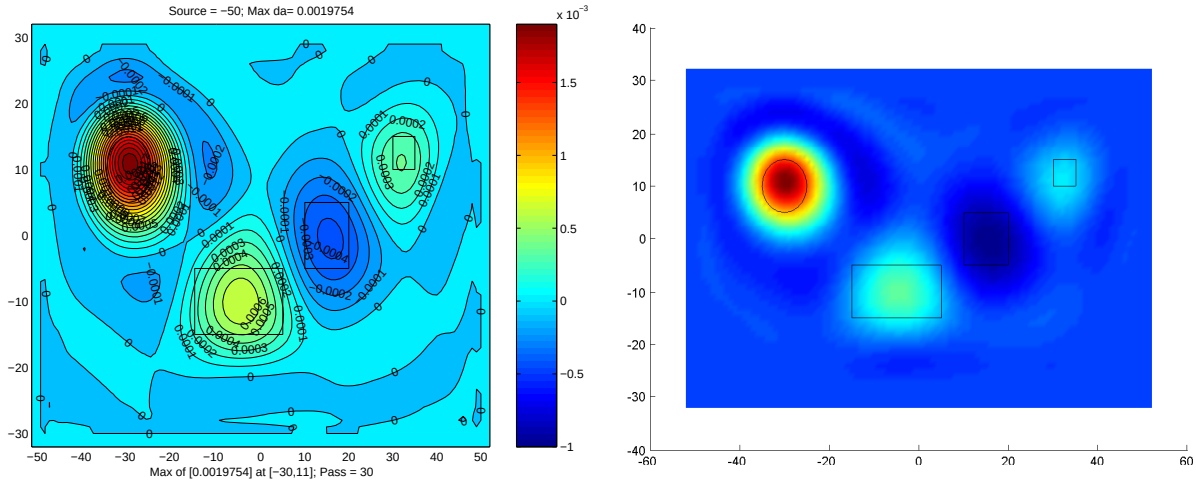

(a) Contour plot of the recovered inclusions.

(b) Plot of the values of the recovered inclusions.

Figure 3: Plots of the recovered inclusions for Example 1. Sources and detectors on all four sides.

6.2 SECOND EXAMPLE: IDC; TOP AND BOTTOM ONLY

Eight sources are used with a CW signal: the top and bottom each having 4. Detectors are placed on the top and bottom sides only. Both transmitted and back-reflected data readings are used. The results are shown in Figure 4, and again appear successful, similar to Example 1.

6.3 THIRD EXAMPLE: IDC; TRANSMITTED DETECTORS ONLY

Eight sources are used with a CW signal: the top and bottom each having 4. For each source, detectors are placed on the opposite side only. The results are shown in Figure 5, and appear successful for the three leftmost inclusions, but miss the smaller inclusion to the far right. In general the results are somewhat degraded from the results of Examples 1 and 2. A small artifact has appeared to the top left of center.

6.4 FOURTH EXAMPLE: IDC; BACK-REFLECTED DETECTORS ONLY

Eight sources are used with a CW signal: the top and bottom each having 4. For each such source, detectors are placed on the same side only (but not close to the source). The results are shown in Figure 6, and appear reasonably successful for the two leftmost of the three positive-valued inclusions. The small positive-valued inclusion to the right is identified rather accurately but its value is not much greater than the background. The negative-valued inclusion 2nd from the right is missed altogether, but this is to be expected given the weak back-reflected interaction for such central locations far from the sides. Two low-valued artifacts have appeared to the top and also to the right of the circular inclusion.

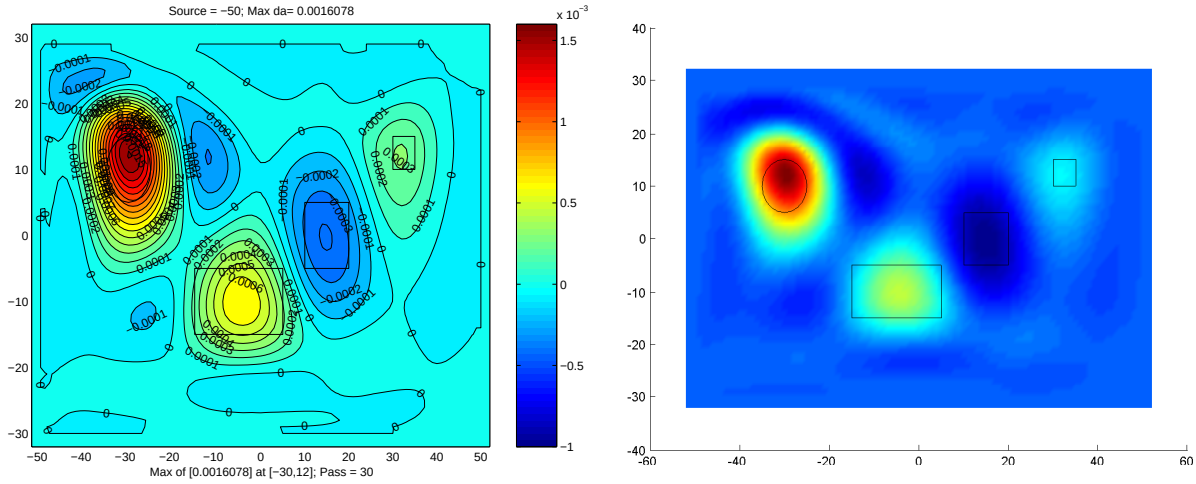

(a) Contour plot of the recovered inclusions.

(b) Plot of the values of the recovered inclusions.

Figure 4: Plots of the recovered inclusions for Example 2. Sources on the top and bottom sides only, using *both transmitted and back-reflected* detector values.

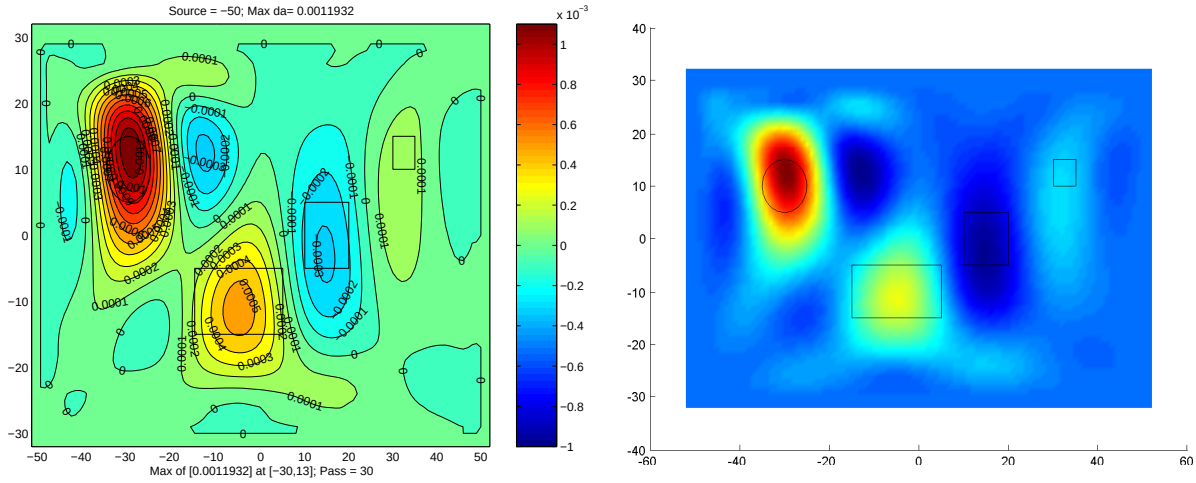

(a) Contour plot of the recovered inclusions.

(b) Plot of the values of the recovered inclusions.

Figure 5: Plots of the recovered inclusions for Example 3. Sources on the top and bottom sides only, using just *transmitted* detector values.

7. CONCLUSIONS

Previous work using the ESM involving either time dependent diffusion tomography [8]-[10],[13] or ground penetrating radar [11]-[12] (with variable modulated frequencies) has been simplified and extended to the application of diffusion tomography in the frequency domain. The results of this process are summarized in the algorithm of Section 4.2 and expanded in Section 5. Important steps in this development were the treatment of the internal singularity at the source x_0, including solving the inverse problem over the extended region G instead of the physical region Ω and the elimination of excessive boundary data requirements. One potential application of this work as it matures would be to the diagnosis of female breast cancer, given a positive result from a mammogram reading. The experimental setup with sources/detectors just on the top or bottom would lend itself well to this type of work.

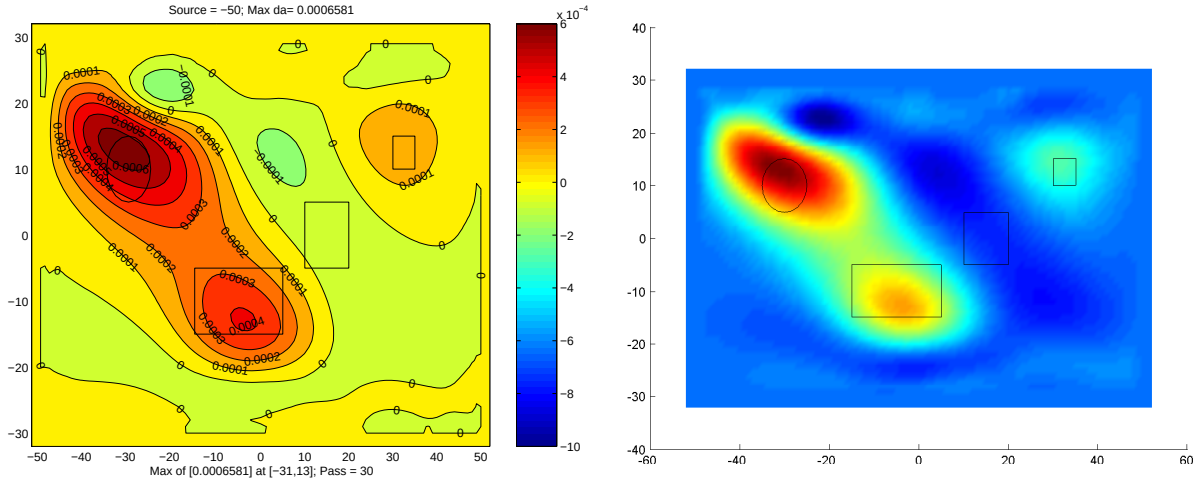

(a) Contour plot of the recovered inclusions.

(b) Plot of the values of the recovered inclusions.

Figure 6: Plots of the recovered inclusions for Example 4. Sources on the top and bottom sides only, using just *back-reflected* detector values.

This preliminary report was limited to the CW case ($\omega = 0$). A particular emphasis of this current work has been in the study of limited data sets. A challenging example with four inclusions, some positive, some negative-valued, and of various magnitudes and shapes was considered with four different data sets for the overdetermined system (9)-(12). The cases of complete data sets, or incomplete data sets limited to the top and bottom, gave the best results with identification of all four inclusions. With transmitted data alone on the top and bottom the inclusion with the smallest capacity [3] (product of size and magnitude) was missed, but the other three inclusions were successfully recovered, including the negative-valued one. With back-reflected data alone on the top and bottom the negative-valued inclusion was completely missed, presumably due to its central location. Interestingly the inclusion with the small capacity in the upper right corner was recovered, but with a small value, similar to the background. The two larger inclusions (one large in area, one in capacity) were easily recovered.

Acknowledgement

This work was supported, in part, by funds and release time provided by The University of North Carolina at Charlotte.

REFERENCES

[1] R. Aronson, Boundary conditions for diffusion of light, *JOSA A* (1995) **12**, 2532-2539.

[2] S. Arridge, Optical tomography in medical imaging, Topical review, *Inverse Problems* (1999), **15**, R41-R93.

[3] G. Bal, Optical tomography for small volume absorbing inclusions, *Inverse Problems* (2003) **19**, 371-386.

[4] P.G. Ciarlet, *The Finite Element Method for Elliptic Problems.* Studies in Mathematics and its Applications, **4**. North-Holland, 1978.

[5] Comsol, *FEMLAB User's Guide*, 2004.

[6] A. George and J.W.H. Liu, *Computer Solution of Large Sparse Positive Definite Systems*, Prentice-Hall, Inc., Englewood Cliffs, New Jersey, 1981.

[7] G.H. Golub and C.F. Van Loan, *Matrix Computations,* The John Hopkins University Press, Baltimore, 1993.

[8] M.V. Klibanov, T.R. Lucas and R. M. Frank, A fast and accurate imaging algorithm in optical/diffusion tomography, *Inverse Problems* (1997), **13**, 1341-1361.

[9] M.V. Klibanov and T.R. Lucas, Numerical solution of a parabolic inverse problem in optical tomography using experimental data, *SIAM J. Appl. Math.* (1999), **59**, 1763-1789.

[10] M.V. Klibanov and T.R. Lucas, Elliptic systems method in diffusion tomography using back-reflected data, *Inverse Problems* (2000), **16**, 199-221.

[11] Y.A. Gryazin, M.V. Klibanov and T.R. Lucas, Numerical solution of a subsurface imaging problem, *SIAM J. Appl. Math.* (2001), **62**, 664-683.

[12] Y.A. Gryazin, M.V. Klibanov and T.R. Lucas, Two numerical methods for an inverse problem for the 2-D Helmholtz equation, *J. Comput. Phys.* (2003), **184**, 122-148.

[13] Y.T. Shih and T.R. Lucas, A new implementation of the elliptic systems method in time dependent diffusion tomography applied to back reflected and transmitted data, *This Proceedings* (2005).